

NICMOS OBSERVATIONS OF THE PRE-MAIN-SEQUENCE PLANETARY DEBRIS SYSTEM HD 98800¹

Frank J. Low, Dean C. Hines & Glenn Schneider

Steward Observatory, The University of Arizona, 933 N. Cherry Ave., Tucson, AZ 85721

flow, dhines, gschneid@as.arizona.edu

ABSTRACT

Spectral energy distributions (SEDs) from 0.4 to 4.7 μ m are presented for the two principal stellar components of HD 98800, A and B. The third major component, an extensive planetary debris system (PDS), emits $> 20\%$ of the luminosity of star B in a blackbody SED at $164 \pm 5K$ extending from mid-IR to millimeter-wavelengths. At 0.95 μ m a preliminary upper limit of < 0.06 is obtained for the ratio of reflected light to the total from star B. This result limits the albedo of the PDS to < 0.3 . Values are presented for the temperature, luminosity, and radius of each major systemic component. Remarkable similarities are found between the PDS and the interplanetary debris system around the Sun as it could have appeared a few million years after its formation.

Subject headings: binaries:visual — circumstellar matter — infrared:stars — stars:individual (HD 98800) — stars:pre-main-sequence

¹Based on observations with the NASA/ESA Hubble Space Telescope obtained at the Space Telescope Science Institute, which is operated by Association of Universities for Research in Astronomy, Incorporated, under NASA contract NAS5-26555.

1. INTRODUCTION

Long known as a visual double with less than $1''$ separation, HD 98800 (SAO 179815; IRAS P11195-2430) was found by *IRAS* to contain the brightest planetary debris system (PDS) in the sky. Now we find that in terms of dimensions, configuration, temperature, and likely origin, this very young PDS bears remarkable similarity to the zodiacal dust bands in our solar system formed and maintained for four billion years by the asteroid families, a phenomenon also discovered by *IRAS* (Low et al. 1984). Recently identified as one of 11 known members of the nearby TW Hydrae Association (Kastner et al. 1997; Webb et al. 1999), the HD 98800 (TWA 4) system is comprised of two similar K dwarfs that have not yet reached the main sequence. Torres et al. (1995) reported that both stars are spectroscopic binaries with periods of 262 (Aa+Ab) and 315 days (Ba+Bb). At a distance of 46.7 ± 6 pc, measured by the *Hipparcos* satellite, the two brightest components of HD 98800 are well resolved by *HST* from 0.4 to $2\mu\text{m}$. See Soderblom et al. (1998) for BVI photometry of the two major components using WFPC2 on *HST*, and for estimates of their masses ($\sim 1 M_{\odot}$) and age (< 10 Myr). From the ground at 4.7 and $9.8\mu\text{m}$, Gehrz et al. (1999) showed that the visual companion (component B) is actually at the center of the PDS with only a small amount of dust possible around star A. Star B lies north of star A by about $0''.8$. Separations of Ab from Aa and of Bb from Ba are of order 1 AU ($0''.02$), and the luminosity of Bb is thought to be greater than that of Ab.

Using the sub-arcsecond resolution and dynamic range in excess of one million afforded by the Near Infrared Camera and Multi-Object Spectrometer (NICMOS) onboard *HST*, we have resolved the two primary components in five bands from 0.95 to $1.9\mu\text{m}$, spanning the peak of their spectral energy distributions. Our objective was to obtain precise relative and absolute photometry of the two stellar components and to search for a halo of scattered or reflected light from the PDS, realizing that all other resolved planetary debris systems scatter and emit about equally. However, based on our predicted inner diameter of < 10 AU and small cross-sectional area for the PDS, we cannot be confident of separating the reflected light from direct starlight.

2. NICMOS OBSERVATIONS AND REDUCTIONS

Table 1 summarizes key observational parameters of the two *HST* orbits (GTO 7232) devoted to these measurements. Spanning 306 days, the two orbits were aimed at obtaining high fidelity “sub-stepped” images using four narrow band filters and one centrally located medium band filter. Four images were planned at each epoch and at each wavelength (Table 1) using a spiral dither pattern (Mackenty et al. 1997) to allow for bad pixel replacement and to improve the spatial sampling (from ~ 2 AU to ~ 1 AU). Unfortunately, in the first orbit only half of the images were obtained due to a pointing error. Care was taken to correct for effects of non-linear response in the detectors, including persistence, for cosmic ray events, and for flat fielding of the images. In-flight flat-field images and the HD 98800 raw images were reduced with in-flight dark frames.

Table 2 summarizes flux densities and their ratios derived from the complete set of 18 images. Our absolute calibrations of the final background subtracted images are based on preliminary photometric calibrations kindly provided by M. Rieke (1999) prior to their publication. Flux densities for magnitude zero stars, accurate to $\pm 3\%$, are listed in Table 2, column 6, to facilitate conversion to magnitudes and for comparisons with other calibrations. When the images are combined, peak signal-to-noise is high ($S/N > 500$), and flat-fields good only to 0.3% dominate the relative photometric errors, while uncertainties in the absolute flux densities are dominated by calibration errors. For completeness we have included the flux densities derived from the B, V and “I” magnitudes reported by Soderblom et al. (1998), and the ratios (B/A) from our reprocessing of their publicly available images.

Precise NICMOS ratios were determined from each calibrated image using the software package IDP3 (Lytle et al. 1999) as follows: a scaled copy of the image was shifted to center star A precisely over star B and the two images were subtracted after varying the scale factor to minimize the residual. Then the process was repeated in reverse order and, finally, the image of star B was divided by that of star A. The residuals were used to determine the error. Subtraction of a PSF-star gave consistent, but noisier results. A similar procedure was used to derive the listed ratios from the WFPC2 images.

3. DISCUSSION

Figure (1) shows the spectral energy distributions of components A and B based on WFPC2 and NICMOS data and the results from Gehrz et al. (1999). For the PDS we include color-corrected Faint Source Catalog flux densities from *IRAS* and measurements at sub-mm wavelengths (see Table 2). Shown in Figure (1a) are blackbody fits to each stellar component and to the PDS. Figure (1b) shows the percentage deviations of the observations of the two stars from the Planck Law. The corresponding blackbody temperatures (T_{BB}) for the two primary stars and for the PDS are included in Table 3, along with errors estimated from the fitting process and from the flux density errors. For comparison, we list effective temperatures for the stars based on the B-V colors from Soderblom et al. (1998) using the Bessell (1979) color-temperature relation, but treating both A and B as single stars. Also, we have attempted to fit these data using model SEDs based on ground-based photometry of K dwarfs of the same spectral types. Unexpectedly, these unpublished models of main sequence K-stars (M. Meyer 1999) do not represent the measured flux densities of A and B short of $2\mu\text{m}$ as well as do the simple blackbody models. However, beyond $2\mu\text{m}$ the SEDs of these stars appear to drop below the simple blackbody model. The luminosities listed in Table 3, derived by integration of the blackbody models, may be high by as much as 3% due to this effect. Because the B-V colors are close to normal for stars with spectral types K5 and K7, we do not include an interstellar extinction correction. Neglecting the uncertainty of the distance, we believe the errors of the luminosity determinations are of order $\pm 5\%$. Taking our measured luminosities and treating our blackbody temperatures as good approximations to

the true effective temperatures, current PMS models¹ give plausible values for mass, but are in conflict with other age indicators.

Using the luminosity and temperature of components A and B their radii were calculated. In neglecting their duplicity we note that this oversimplification is more significant for B than for A (see Soderblom et al. 1996). The values in Table 3 show that the cooler star, B, is slightly larger than star A, a result well within the precision of the relative measurements involved. Pre-main sequence stars may well have this property. However, when both components of star B are considered, they each can have radii smaller than that of star Aa (Ab is almost negligible), and as previously noted, some portion of the power emitted by Ba and Bb will be reflected by the PDS adding to the star’s apparent luminosity. Figure 1 shows that there are slight differences between the two primary components when compared in detail relative to their respective blackbodies. Also, star A varies at all wavelengths by as much as a few percent and significant coronal activity has been reported (e.g. Fekel & Bopp 1993; Henry & Hall 1994).

At $0.95\mu\text{m}$, where our resolution is highest, we have been unable to detect starlight reflected by the PDS. From the residuals of the flux-scaled PSF subtraction, we place a tentative upper limit of $< 6\%$ for the reflected light relative to the direct emission from Ba+Bb. These residuals have been compared to quantitative predictions based on a simplified geometrical model of the IR source convolved with star A (which serves as the PSF). From Table 3 we see that the power emitted in our direction by the PDS divided by the total power emitted by the Ba+Bb systemic components and reflected from the PDS is 0.19. Therefore, at $0.95\mu\text{m}$ we have placed an upper limit on the albedo of the reflecting material of 0.3, well within the range expected for such material. Asteroids have albedos that are generally lower than 0.3 [see results from *IRAS* reported by Tedesco et al. (1989)]. Note also that we have direct observational evidence from the work of Skinner, Barlow & Justtanont (1992) that the emitting material contains silicates. However, in our filters we see no indication of coloration of the stellar emission from component B as might be caused by reflection from the PDS. This suggests that the albedo is low at all bands from 0.4 to $2\mu\text{m}$.

Next, we must explain how a circumstellar envelope can form and be maintained over millions of years with geometry, opacity, and stability sufficient to produce the system that we observe. When Zuckerman & Becklin (1993) reported the extraordinarily high value of $L_{\text{IR}}/L_{\text{bol}}$ for HD 98800, they pointed out that the lifetime of a circumstellar dust cloud thick enough to absorb 15% or more of the stellar emission would quickly evolve into a thin disk. Consider the case of a failed terrestrial planet of sufficient mass to form dense “dust bands” which overlap and fill in a belt subtending 20% of the celestial sphere around the stars. The required range of orbital inclinations is -12° to $+12^\circ$. In the solar system the dust bands lie 10° above and below the zodiacal plane, and are constantly replenished by collisional erosion of asteroids in those same orbits. The much larger quantity of dust in the HD 98800B planetary debris system follows from

¹<http://www-astro.phast.umass.edu/data/tracks.html>

its recent formation

Just as we calculated the radii of the stars, we have also calculated an “equivalent” radius for the material orbiting around star B, even though in projection the IR source, clearly, is not circular in shape. The result listed in Table 3, 2 AU, is consistent with our proposed geometry of the PDS, and constrains that portion of the belt that is visible directly. The actual radii of the inner debris orbits, about 4.5 AU, can be predicted because the material must be in radiative equilibrium with the measured emission of the two central stars. In the solar system, where the corresponding temperatures are 200 to 250 K, the dust is optically thin, of order 10^{-8} , and its emission follows a blackbody at least out to $100\mu\text{m}$.

In HD 98800B the dust opacity remains high from 7 to at least $1000\mu\text{m}$, but we find no indication of attenuation of light from star B. This implies that the orbital plane of the dust system is inclined to our line of sight by more than 12° . The most likely value is near 45° since the emitting area must equal that of the equivalent disk, ~ 12 sq. AU. Because most of the 165 K emitting surface is obscured by colder particles in larger orbits, the actual ratio of IR to optical luminosity is probably higher than the observed ratio of 0.19 reported here. Clearly, the IR emission is not isotropic. Using the predicted 4.5 AU inner radius of the belt, an equivalent thickness of 1 mm, and terrestrial density, a rough estimate of minimum mass is $0.6 M_\oplus$.

In conclusion, we now have enough information about the stars in HD 98800 to test, and perhaps improve, models of PMS dwarfs. We can also construct plausible models of recently formed planetary debris systems with interesting similarities to our own planetary system. We note that as yet no other examples of very young systems of this type have been found, indicating that the lifetime of this optically thick phase is probably rather short. Future observations using adaptive optics on the largest telescopes and space missions such as NGST should resolve both the thermal and reflected components of the PDS around HD 98800B. Infrared surveys now in progress and in the planning stage with SIRTf should provide new and better means of locating planetary debris systems, thus providing an answer to the question of how often terrestrial planets are formed.

Valuable assistance from our colleagues, M. Meyer, M. Rieke, D. McCarthy and E. Becklin is much appreciated, and we thank A. Shultz, D. Golombek, P. Stanley, and I. Dashevsky for their help at STScI. This work is supported by NASA grant NAG5-3042 to the NICMOS instrument definition team.

REFERENCES

- Bessel, M.S. 1979, PASP, 91, 383
Bessel, M.S., Castelli, F. & Plez, B. 1998, A&A, 333, 231
Fekel, F. C. & Bopp, B. W. 1993, ApJ, 419, L89

- Gehrz, R. D., Smith, N. , Low, F. J., Krautter, J. , Nollenberg, J. G. & Jones, T. J. 1999, ApJ, 512, L55
- Henry, G. W. & Hall, D. S. 1994, ApJ, 425, L25
- Kastner, J.H., Zuckerman, B., Weintraub, D.A. & Forveille, T. 1997, Science, 277, 67
- Low, F. J., et al. 1984, ApJ, 278, L19
- Lytle, D., Stobie, E., Ferro, A., & Barg, I. 1999, ASP Conf. Ser., Astronomical Data Analysis Software and Systems 8, ed. D. Mehringer, R. Plante, & D. Roberts (San Francisco: ASP), in press
- Mackenty, J. W., et al, 1997, NICMOS Instrument Handbook, Version 2.0, (Baltimore: STScI).
- Rucinski, S. 1993, IAUC, 5788
- Skinner, C.J., Barlow, M.J. & Justtanont 1992, MNRAS, 255, 31P
- Soderblom, D. R., Henry, T. J., Shetrone, M. D., Jones, B. F. & Saar, S. H. 1996, ApJ, 460, 984
- Soderblom, D. R., et al. 1998, ApJ, 498, 385
- Stern, S.A., Weintraub, D.A. & Festou, M.C. 1993, IAUC 6003
- Sylvester, R. J., Skinner, C. J., Barlow, M. J. & Mannings, V. 1996, MNRAS, 279, 915
- Tedesco, E.F., Matson, D.L. & Veeder, G.J. 1989, in Asteroids II, R.P. eds. Binzel, T. Gehrels & M.S. Matthews, (University of Arizona Press:Tucson)
- Torres, G., Stefanik, R.P., Latham, D.W. & Mazeh, T. 1995, ApJ, 452, 870
- Webb, R. A., Zuckerman, B., Platais, I., Patience, J., White, R. J., Schwartz, M. J. & McCarthy, C. 1999, ApJ, 512, L63
- Zuckerman, B. & Becklin, E.E. 1993, ApJ, 406, L25

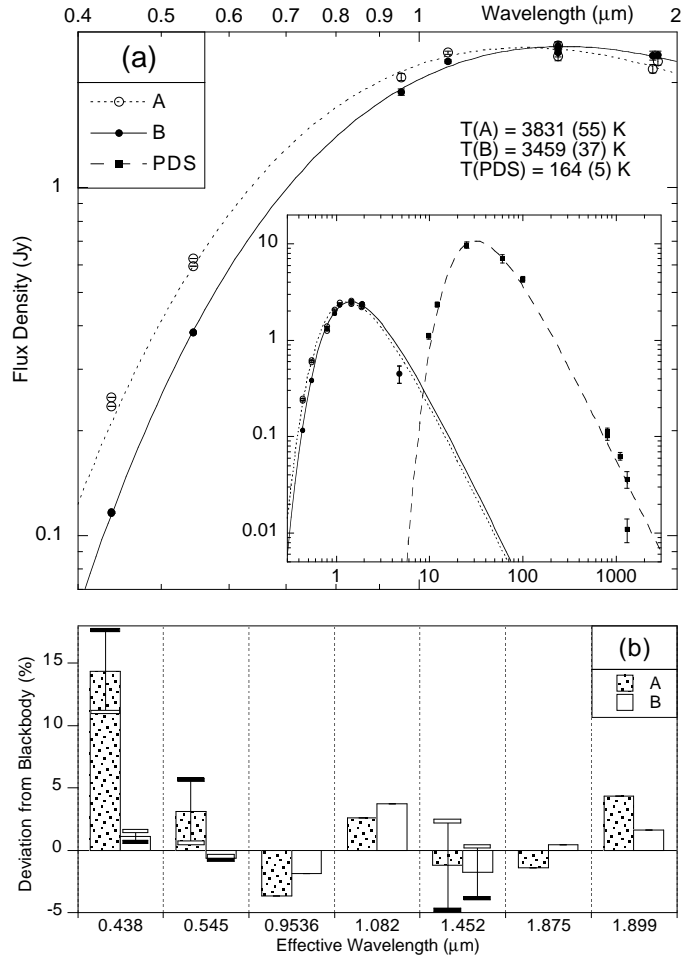


Fig. 1.— (a) SEDs of primary components with blackbody fits. Expanded view shows the measurements used for the fits to A & B. (b) Spectral and temporal deviations of mean flux densities from blackbody fits. First epoch indicated by black (see Table 2).

Table 1. NICMOS Observation Log

| Date (UT) | Filter | Mode | Exposure (sec) | Dither (pixels) | $\lambda/2D^a$ (") | Frames |
|--------------|--------|--------|-------------------|--------------------|-----------------------|--------|
| 1997 Jul 3 | F108N | STEP2 | 67.78 | 50.5 | 0.0465 | 2 |
| 1997 Jul 3 | F145M | SCAMRR | 7.30 | 50.5 | 0.0624 | 2 |
| 1997 Jul 3 | F187N | STEP2 | 59.82 | 50.5 | 0.0806 | 2 |
| 1998 May 1 | F095N | STEP2 | 135.56 | 30.5 | 0.0410 | 4 |
| 1998 May 1 | F145M | SCAMRR | 16.24 | 30.5 | 0.0624 | 4 |
| 1998 May 1 | F190N | STEP2 | 135.56 | 30.5 | 0.0816 | 4 |

^aNIC1 pixel scale = $0.0432'' \times 0.0432''$, 1.0 AU = $0.021''$

TABLE 2
PHOTOMETRY OF HD 98800

| Instrument | Date (UT) | Filter/Band | λ_{Eff} (μm) | $\Delta\lambda$ (μm) | $m = 0^a$ (Jy) | A (σ) (Jy) | B (σ) (Jy) | B/A (σ) ^b | Refs. |
|------------|---------------|-------------------|---|--------------------------------------|-------------------|------------------------|------------------------|-------------------------------|-------|
| WFPC2 | 1996 Jan 5 | F438W (B) | 0.438 | 0.0464 | 4063 | 0.25 (...) | 0.12 (...) | 0.48 (0.01) | 1 |
| WFPC2 | 1996 Jan 5 | F545W (V) | 0.545 | 0.1222 | 3636 | 0.63 (...) | 0.38 (...) | 0.58 (0.01) | 1 |
| WFPC2 | 1996 Jan 5 | F953N (I) | 0.798 | 0.0052 | 2416 | 1.39 (...) | 1.31 (...) | 0.94 (0.01) | 1 |
| WFPC2 | 1996 Mar 3 | F439W (B) | 0.438 | 0.0464 | 4063 | 0.24 (...) | 0.12 (...) | 0.49 (0.01) | 1 |
| WFPC2 | 1996 Mar 3 | F555W (V) | 0.545 | 0.1222 | 3636 | 0.59 (...) | 0.38 (...) | 0.65 (0.02) | 1 |
| WFPC2 | 1996 Mar 3 | F953N (I) | 0.798 | 0.0052 | 2416 | 1.25 (...) | 1.31 (...) | 0.96 (0.01) | 1 |
| NICMOS | 1997 Jul 3 | F108N | 1.0816 | 0.0094 | 1805 | 2.443 (0.017) | 2.304 (0.014) | 0.943 (0.007) | 2 |
| NICMOS | 1997 Jul 3 | F145M | 1.4524 | 0.1965 | 1272 | 2.380 (0.005) | 2.442 (0.005) | 1.026 (0.002) | 2 |
| NICMOS | 1997 Jul 3 | F187N | 1.8748 | 0.0188 | 825 | 2.193 (0.011) | 2.392 (0.012) | 1.091 (0.005) | 2 |
| NICMOS | 1998 May 1 | F095N | 0.9536 | 0.0088 | 2010 | 2.076 (0.007) | 1.882 (0.007) | 0.904 (0.004) | 2 |
| NICMOS | 1998 May 1 | F145M | 1.4524 | 0.1965 | 1272 | 2.559 (0.003) | 2.549 (0.003) | 0.996 (0.001) | 2 |
| NICMOS | 1998 May 1 | F190N | 1.8986 | 0.0174 | 808 | 2.301 (0.007) | 2.404 (0.007) | 1.045 (0.003) | 2 |
| TIMMI | 1996 April 5 | M | 4.71 | 0.99 | 165.4 | 0.45 (0.09) | 0.45 (0.09) | 1.00 (0.15) | 3 |
| TIMMI | 1996 April 5 | N2 | 9.78 | 1.29 | 40.3 | 0.30 (0.07) | 1.10 (0.07) | 3.70 (0.56) | 3 |
| IRAS | 1983 | 12 μm | 12 | 7.5 | 28.3 | ... | 2.36 (0.14) | ... | 2 |
| IRAS | 1983 | 25 μm | 25 | 11 | 6.73 | ... | 9.74 (0.78) | ... | 2 |
| IRAS | 1983 | 60 μm | 60 | 40 | 1.19 | ... | 7.05 (0.70) | ... | 2 |
| IRAS | 1983 | 100 μm | 100 | 37 | 0.43 | ... | 4.31 (0.30) | ... | 2 |
| JCMT | 1992 Feb | 800 μm | 800 | ... | ... | ... | 0.111 (0.012) | ... | 4 |
| JCMT | 1993 April 25 | 800 μm | 800 | ... | ... | ... | 0.102 (0.010) | ... | 5 |
| JCMT | 1992 Feb, Mar | 1.1mm | 1100 | ... | ... | ... | 0.063 (0.006) | ... | 4 |
| IRAM | 1993 April 17 | 1.3mm | 1300 | ... | ... | ... | 0.036 (0.007) | ... | 6 |
| JCMT | 1994 April | 1.3mm | 1300 | ... | ... | ... | 0.011 (0.003) | ... | 4 |

^aBased on: Bessel, Castelli & Plez 1998, NICMOS IDT, Personal Comm., IRAS Explanatory Supplement

^bMeasured from images independent of photometric calibration.

REFERENCES.—(1) Soderblom et al. 1998; (2) This work; (3) Gehrz et al. 1999; (4) Sylvester et al. 1996; (5) Rucinski 1993; (6) Stern, Weintraub & Festou 1993

Table 3. Derived properties of HD 98800

| Comp. | Sp. ^a | T _{eff} (B-V) ^b (K) | T _{BB} (K) | L ^c (L _⊙) | R ^d (R _⊙) | Mass (M _⊕) |
|-------|------------------|--|------------------------|-------------------------------------|-------------------------------------|---------------------------|
| A | K5 | 4100 | 3831 (55) | 0.63 (0.03) | 1.94 (0.06) | ... |
| B | K7 | 3500 | 3459 (37) | 0.57 (0.03) | 2.13 (0.06) | ... |
| PDS | ... | ... | 164 (5) | 0.11 (0.01) | 417 (34) | 0.6 |
| PDS | ... | ... | ... | 0.19L _{StarB} | 1.94 AU | ... |

^aBased on B-V colors from Soderblom et al. (1998)

^bEffective temperature based on B-V colors.

^cLuminosity assuming isotropy and d = 46.7 pc (Fig. 1)

^dThe effective/equivalent radius of a blackbody of temperature T_{BB}.